# Supporting Information

## Experimental section

**General Information.** All chemical reagents and solvents were procured commercially and were used without further purifications unless otherwise stated. Hexahydroxybenzene and tetrahydroxy-1,4-benzoquinone hydrate were purchased from TCI China. $Mn(CH_3COO)_2 \cdot 4H_2O$ (99.99%), RbCl (99%) and CsCl (99.998%) were purchased from Alfa Aesar China Co. Ltd. The solvents were degassed by the Freeze-Thaw method. All MOFs were obtained by solvothermal reactions.

**Synthesis of MnHHB.** Under nitrogen conditions, 46 mg HHB (0.26 mmol) and 127.4 mg $Mn(CH_3COO)_2 \cdot 4H_2O$ (0.52 mmol) were dissolved in 20 ml degassed water in a 50ml Teflon vessel. After the vessel was placed in an autoclave, the autoclave was put in an oven then began to heated to 120°C for 48 hours. When the temperature was decreased to room temperature, the autoclave was taken out and the powder was filtered and washed with water (3 x 50 ml) and EtOH (2 x 50 ml) and then, the dark-blue powder was dried at 45°C in the vacuum oven for 6 hours, preparing for the subsequent measurements. Yield: 50 mg (79%). Anal. Calcd for $Mn_5C_{12}O_{13.5}H_3$: C, 22.60; H, 0.47; Mn, 43.07%. Found: C, 24.72; H, <0.3; Mn, 44.60%. CCDC 2115127 contains the supplementary crystallographic data for MnHHB. The data can be obtained free of charge from The Cambridge Crystallographic Data Centre via www.ccdc.cam.ac.uk/structures.

**Synthesis of MnRbTHBQ.** In a Nitrogen-filled glovebox, 45 mg THBQ (0.26 mmol) were dispersed in 10 ml degassed water sufficiently in a 50 ml Teflon vessel, 10 ml of degassed water dissolved with 127.4 mg $Mn(CH_3COO)_2 \cdot 4H_2O$ (0.52 mmol) and 628.68 mg RbCl (5.2 mmol ) was added into the vessel. Then, the vessel was sealed and placed in an oven heated for 48 hours at 120°C. After cooling to room temperature, the powder was filtered and washed with water (3 x 60 ml), EtOH (2 x 50 ml) and the powder was dried at 45°C in the vacuum oven for about 6 hours, preparing for the subsequent measurements. Yield: 40 mg (52%). Anal. Calcd for $Mn_3Rb_2C_{12}O_{18}H_{12}$: C, 18.48; H, 1.55; Mn, 21.13; Rb, 21.92 %. Found: C, 23.42; H, 0.92; Mn, 24.39; Rb, 22.31 %.

**Synthesis of MnCsTHBQ.** The preparation of MnCsTHBQ was similar with MnRbTHBQ. Under nitrogen conditions, 45 mg THBQ (0.26 mmol) were dispersed in

10 ml degassed water in a 50 ml Teflon vessel. Meanwhile, 127.4 mg $Mn(CH_3COO)_2{\cdot}4H_2O$ (0.52 mmol) and 437.7 mg CsCl (2.6 mmol ) were dissolved in 10 ml degassed water, which was added into the 50 ml vessel, mixed with THBQ dispersion. After sealed into an autoclave, the container was put into an oven heated for 48 hours at 120°C. The powder was filtered and washed with water (3 x 50 ml), EtOH (2 x 50 ml) and dried at 45°C in the vacuum oven for about 6 hours, preparing for the subsequent measurements. Yield: 36 mg (41%). Anal. Calcd for $Mn_3Cs_2C_{12}O_{18}H_{12}$: C, 16.48; H, 1.38; Mn, 18.84; Cs, 30.38 %. Found: C, 22.48; H, 1.02; Mn, 21.88; Cs, 28.15 %. The differences of the theoretical and experimental data could because the impurities in the MOFs and the hydrolysis of alkali metal ions.

**Component analysis.** The Flash EA 1112 (Thermo Fisher Scientific) was used to analyze the percentages of carbon and hydrogen. The content of Mn was analyzed by inductively coupled plasma-optical emission spectroscopy (ICP-OES, iCAP 6300 Radial, Thermo Scientific). For ICP-OES measurements, the samples were prepared by dissolving them into fuming nitric acid, and the solution was diluted to a volumetric flask with Milli-Q water. XPS was performed on the AXIS Ultra-DLD ultrahigh vacuum photoemission spectroscopy system (Kratos Co.) with a monochromatic Al Kα source (1486.6 eV). Saturated carbon (C-C) C 1s peak at 284.8 eV was used to internally calibrate the XPS.

**Synchrotron powder XRD and structure determination.** The diffraction pattern of collected at the beamline BL14B1 at Shanghai Synchrotron Radiation Facility (λ = 0.69003 Å) was indexed using the N-TREOR09 program integrated in EXPO2014[1] package based on the first 20 intensive peaks. The initial cell parameters were refined by le Bail algorithm using the program Jana2006[2]. Background, zero-point, profile shape and asymmetry correction were refined together using program Jana2006. The structure of the complexes were solved using the charge flipping algorithm implemented in the computer program Superflip[3]. All non-hydrogen atoms could be automatically located from the electron density map. The final structure models were both refined by the Rietveld method using the program Jana2006. TEM images were obtained by using a JEM 2100F (JEOL) TEM with an accelerated voltage of 120 kV.

**Electrical conductivity measurements.** The electrical conductivities were measured via a four-probe method by using a KEITHLEY 2002 Multimeter (Keithley Instrument Inc.). About 18 mg powder was compressed into a cuboid pellet, and then the pellets

were connected with four probes by conductive adhesive, which can be used for measurement after about 3 hours. Arrhenius equation $\sigma = \sigma_0 \exp(-Ea/k_BT)$ ($\sigma$ is the conductivity, $\sigma_0$ is a prefactor, $k_B$ is the Boltzmann constant with the value of $1.38 \times 10^{-23} J \cdot K^{-1}$ and T is the absolute temperature).

**UV-vis-NIR diffuse reflectance spectroscopic characterization**. The spectra between 220 to 1400 nm were collected with a UV-2000 (SHIMADZU) spectrophotometer at room temperature. Moderate sample powder was spread on the non-absorbing matrix, barium sulfate powder.

**Raman spectroscopic characterization.** Raman spectra were recorded at room temperature by using a LabRAM HR Evolution (HORIBA) Raman spectrometer with an excitation wavelength of 532 nm. Moderate powder was mixed with spectrum pure KBr and then, it was compressed into a flake for measurement.

**Theoretical calculations.** The spin-polarized electronic band structure calculations of MnHHB were performed using the Vienna ab initio simulation package (VASP) with the generalized gradient approximation (GGA) of Perdew-Burke-Ernzerhof (PBE)[4]. The projector augmented wave (PAW) method was used to describe the electron-ion interaction[5]. A cutoff energy of 500 eV was used for the plane-wave basis set in all calculations and the energy convergence threshold was $10^{-5}$ eV. The optimization calculations were conducted with a 6×6×4 k-mesh of the Monkhorst-Pack sampling scheme based on a 1×1×2 supercell[6].

## Supporting figures and tables

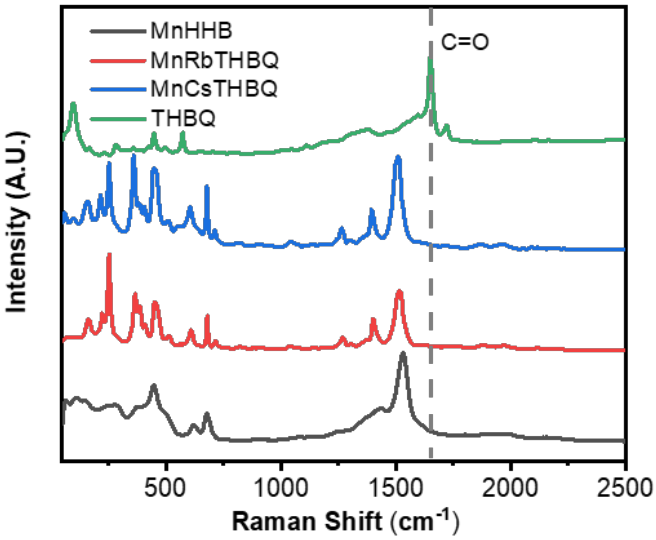


Figure S1. The Raman spectra of MnHHB and MnRbTHBQ, MnCsTHBQ and THBQ. The peak at 1652 $cm^{-1}$ was assigned to C=O in THBQ and it disappeared in bimetallic MOFs, confirming the coordination between O and metal ions[7].

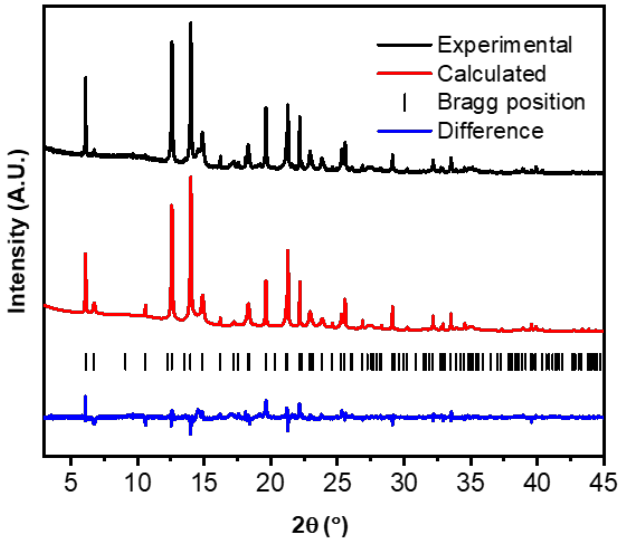


Figure S2. Rietveld refinement of the MnHHB PXRD data.

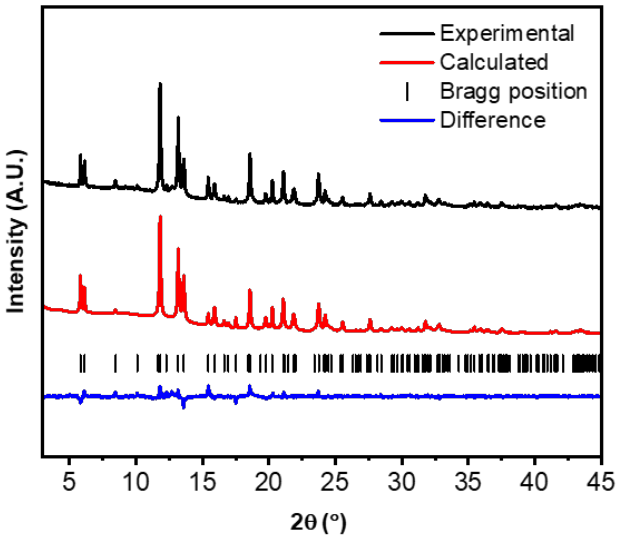


Figure S3. Rietveld refinement of the MnRbTHBQ PXRD data.

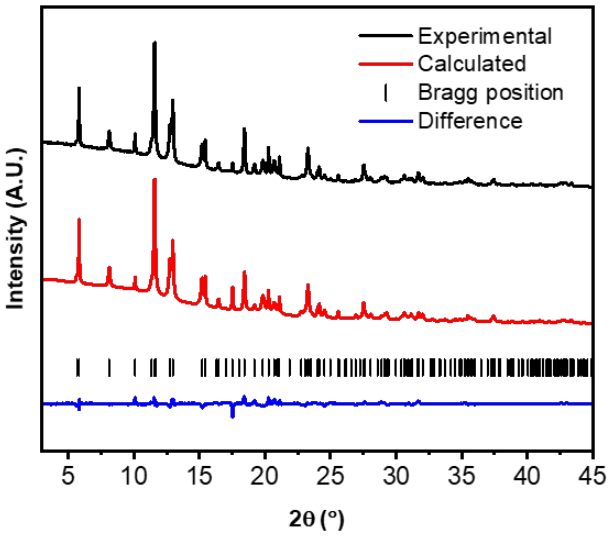


Figure S4. Rietveld refinement of the MnCsTHBQ PXRD data.

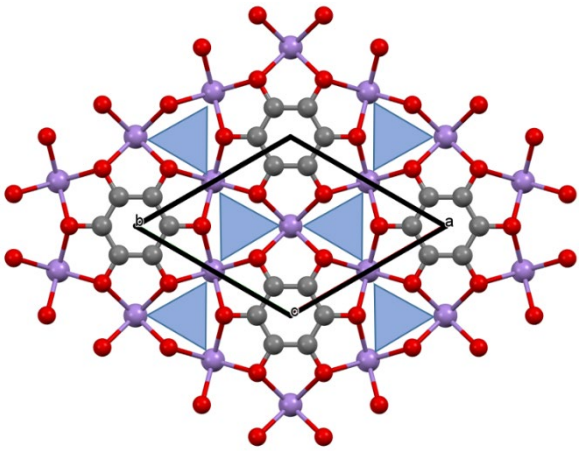

Figure S5. Top view along c-axis of the Kagome lattice of the 2D layered [$Mn1_3C_6O_6$]n (Mn2 atoms locate at the center place of the grey triangular area).

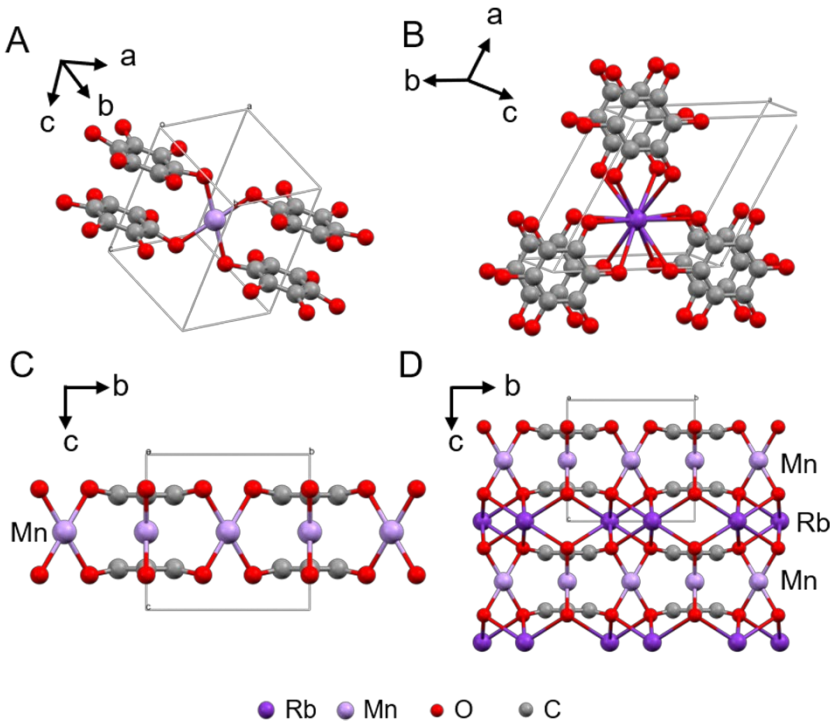


Figure S6. Crystal structure of MnRbTHBQ. (A) The metal-ligand connectivity of the Mn atoms and (B) Rb atoms. (C) The extended ligand dimers in MnRbTHBQ. (D) The 3D network structure of MnRbTHBQ (O atoms from $H_2O$ are omitted for clarity).

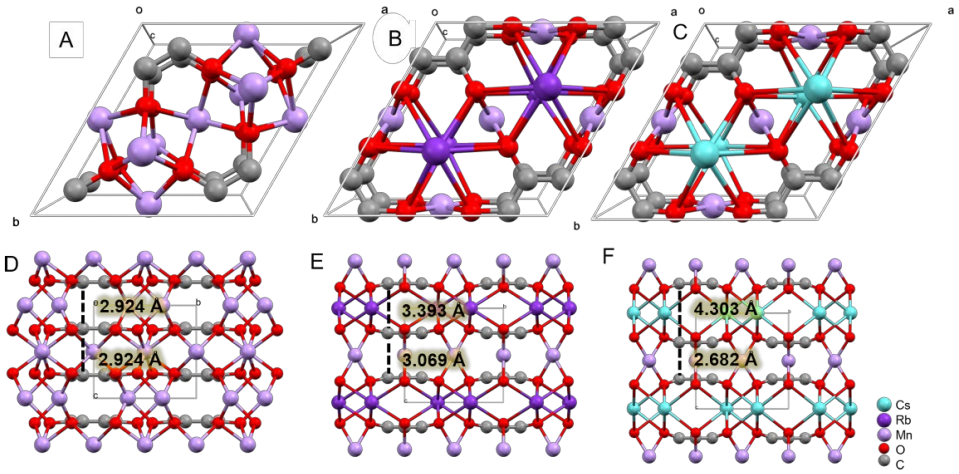


Figure S7. (A-C) The unit cell of MnHHB, MnRbTHBQ and MnCsTHBQ. (D-F) The illustration of the distances of C6 rings for MnHHB, MnRbTHBQ and MnCsTHBQ, respectively.

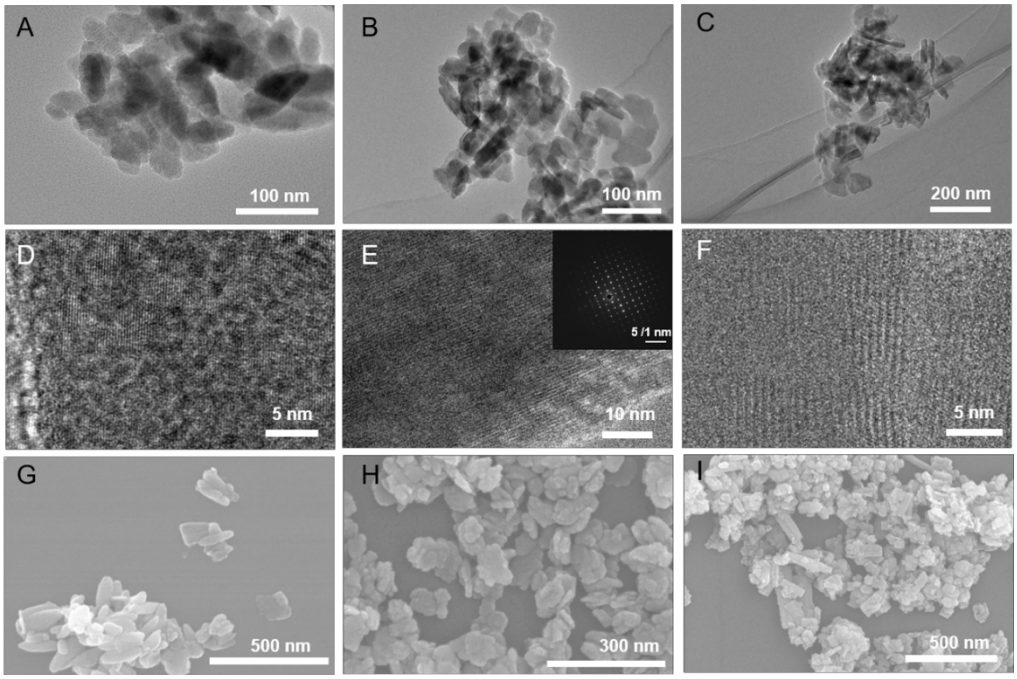


Figure S8. The transmission electron microscopy (TEM) images of MnHHB (A), MnRbTHBQ (B), MnCsTHBQ (C) and the high-resolution TEM images of MnHHB (D), MnRbTHBQ (E), MnCsTHBQ (F), (E) inset is the selected area electron diffraction (SAED) pattern. The scanning electron microscopy (SEM) images of MnHHB (D), MnRbTHBQ (E), MnCsTHBQ (F). The morphologies of MnHHB and MnRbTHBQ exhibited fusiform and nanosheet morphology, respectively. MnCsTHBQ displayed various morphologies of nanosheets and nanorods.

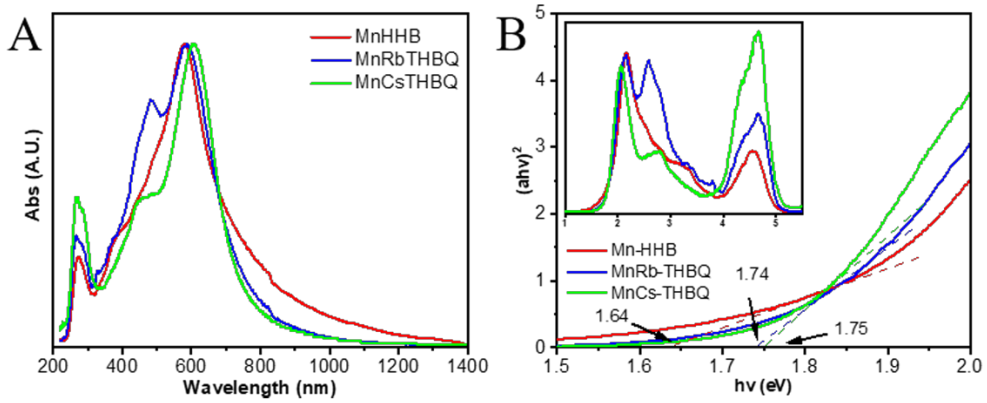


Figure S9. (A) The UV−vis−NIR diffuse reflectance spectroscopies of MnHHB, MnRbTHBQ, MnCsTHBQ. (B) Plots of $(\alpha h\nu)^2$ versus photon energy hν of MnHHB, MnRbTHBQ, MnCsTHBQ. The UV−vis−NIR diffuse reflectance spectroscopies were similar to each other, indicating similar electronic transitions in these three MOFs.

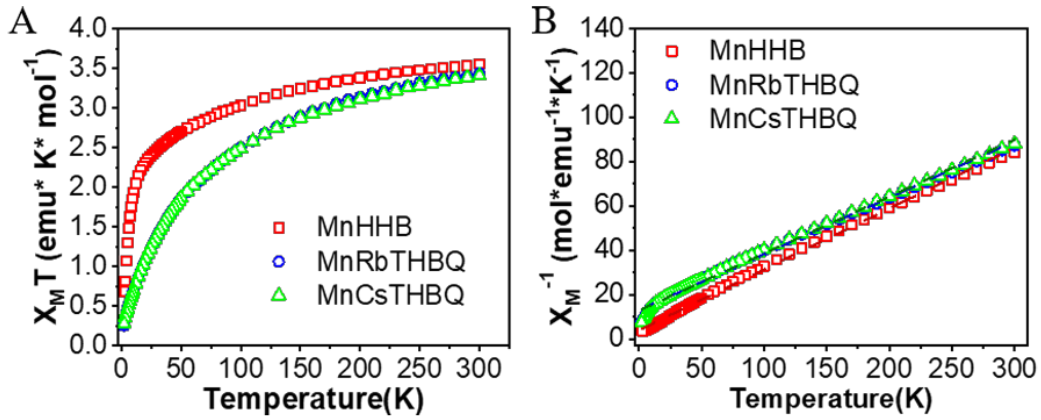


Figure S10. (A) The $\chi_M T$ vs. T curves of MnHHB, MnRbTHBQ and MnCsTHBQ. (B) The $\chi_M^{-1}$ vs. T curves of MnHHB, MnRbTHBQ and MnCsTHBQ and the dotted lines are Curie-Weiss fitting lines.

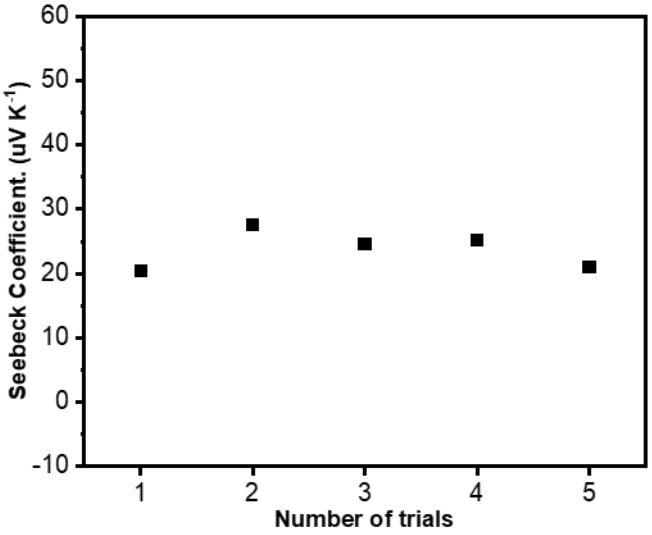


Figure S11. The seebeck coefficient (S) of MnHHB at 300K and the average value was 23.8 μV $K^{-1}$, the power factor (PF = $\sigma S^2$) was $3x10^{-4}$ μW $m^{-1}$ $K^{-2}$.

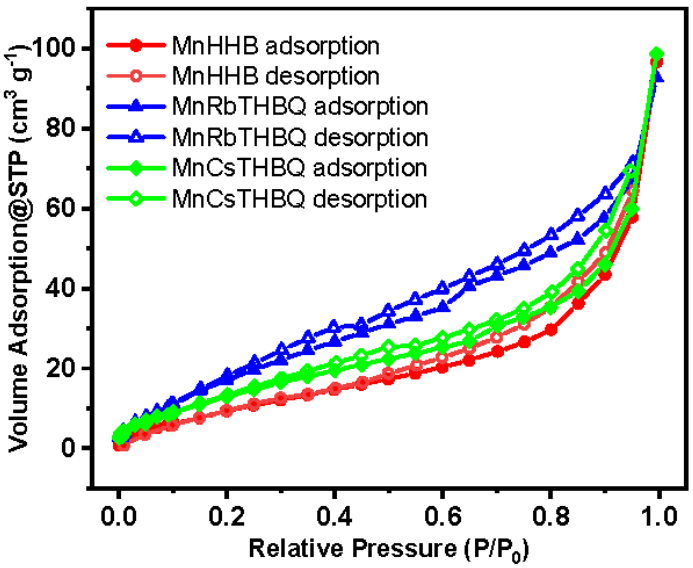


Figure S12. $N_2$ adsorption-desorption isotherms of MnHHB, MnRbTHBQ and MnCsTHBQ at 77 K. The Brunauer-Emmett-Teller (BET) surface area of MnHHB, MnRbTHBQ and MnCsTHBQ was 44.47 $m^2$ $g^{-1}$, 54.20 $m^2$ $g^{-1}$, 37.78 $m^2$ $g^{-1}$, respectively. The low surface areas could because that the dense structures.

Table S1. The crystal information about MnHHB, MnRbTHBQ and MnCsTHBQ.

| | **MnHHB** | **MnRbTHBQ** | **MnCsTHBQ** |
|---|---|---|---|
| **Formula** | $Mn_5C_{12}O_{12}$ | $Mn_3Rb_2C_{12}O_{18}H_{12}$ | $Mn_3Cs_2C_{12}O_{18}H_{12}$ |
| **Formula weight** | 610.81 | 779.96 | 874.84 |
| **Crystal system** | Hexagonal | Hexagonal | Hexagonal |
| **Space group** | P6/mmm | P6/mmm | P6/mmm |
| **a (Å)** | 7.4696 | 7.851 | 7.844 |
| **b (Å)** | 7.4696 | 7.851 | 7.844 |
| **c (Å)** | 5.847 | 6.462 | 6.985 |
| **α** | 90 | 90 | 90 |
| **β** | 90 | 90 | 90 |
| **γ** | 120 | 120 | 120 |
| **V ($Å^3$)** | 282.526 | 344.943 | 372.196 |
| **Wavelength (Å)** | 0.690026 | 0.690026 | 0.690026 |
| **Rwp** | 7.44 | 7.42 | 3.40 |
| **Rp** | 5.19 | 5.10 | 2.01 |
| **GOF** | 3.16 | 3.29 | 1.89 |

Table S2. The distances of C6 rings in MnHHB, MnRbTHBQ and MnCsTHBQ.

| | **MnHHB** | **MnRbTHBQ** | **MnCsTHBQ** |
|---|---|---|---|
| **Z** | Mn1 | Mn | Mn |
| **d (C6…Z…C6)** | 2.924 Å | 3.069 Å | 2.682 Å |
| **Y** | Mn2 | Rb | Cs |
| **d (C6…Y…C6)** | 2.924 Å | 3.393 Å | 4.303 Å |

Table S3. The comparison of the structures of MnTHBQ, MnHHB, MnRbTHBQ and MnCsTHBQ.

| | **Mn-THBQ** | **MnHHB** | **MnRbTHBQ** | **MnCsTHBQ** |
|---|---|---|---|---|
| **Crystal system** | Cubic | Hexagonal | Hexagonal | Hexagonal |
| **Space group** | Pm-3 | P6/mmm | P6/mmm | P6/mmm |
| **a (Å)** | 10.699 | 7.4696 | 7.851 | 7.844 |
| **b (Å)** | 10.699 | 7.4696 | 7.851 | 7.844 |
| **c (Å)** | 10.699 | 5.847 | 6.462 | 6.985 |
| **α** | 90 | 90 | 90 | 90 |
| **β** | 90 | 90 | 90 | 90 |
| **γ** | 90 | 120 | 120 | 120 |

Table S4. The summary of conductivities of THBQ/HHB-based MOFs.

| | $\sigma_{300K}$ **(S cm$^{-1}$)** | $\sigma_{400K}$ **(S cm$^{-1}$)** |
|---|---|---|
| **MnHHB** | 5.4 x$10^{-3}$ | 1.8 x $10^{-2}$ |
| **MnRbTHBQ** | 1.6 x $10^{-7}$ | 7.5 x $10^{-6}$ |
| **MnCsTHBQ** | 1.2 x $10^{-8}$ | 4.8 x $10^{-7}$ |
| **FeTHBQ**[8] | 2.7 x $10^{-4}$ | 2.7 x $10^{-3}$ |
| **CoTHBQ**[8] | 6.0 x $10^{-8}$ | 5.4 x $10^{-6}$ |
| **MnTHBQ**[8] | 3.5 x $10^{-8}$ | 3.7 x $10^{-6}$ |
| **CuTHQ/CuHHB**[9] | 7.3 x $10^{-8}$ | 2.0 × $10^{-6}$ (378 K) |
| **FeTHQ**[10] | 3.3 x$10^{-3}$ | - |

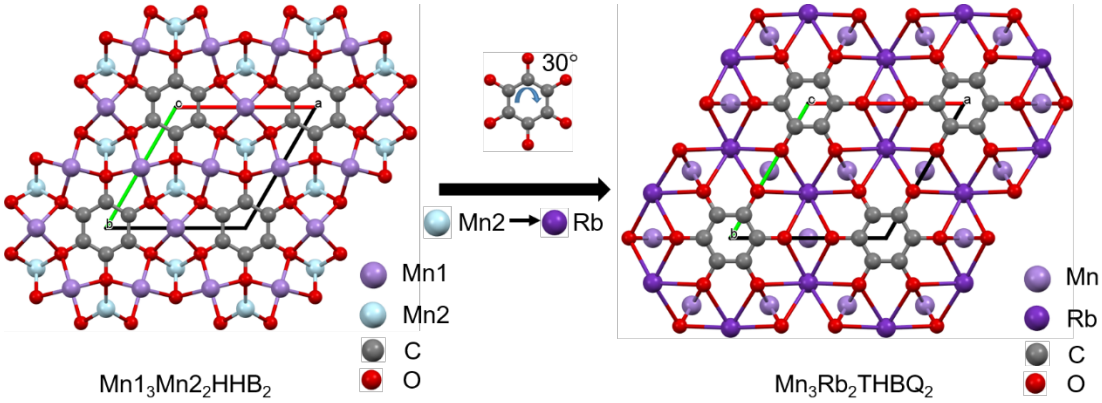


Scheme S1. Comparison of the structure of MnHHB and MnRbTHBQ along c-axis.


[1] A. Altomare, M. Camalli, C. Cuocci, C. Giacovazzo, A. Moliterni, R. Rizzi, *J. Appl. Crystallogr.* **2009**, *42*, 1197-1202.

[2] P. Václav, D. Michal, P. Lukáš, *Z Kristallogr. Cryst. Mater.* **2014**, *229*, 345-352.

[3] L. Palatinus, G. Chapuis, *J. Appl. Crystallogr.* **2007**, *40*, 786-790.

[4] (a) G. Kresse, J. Furthmuller, *Phys. Rev. B* **1996**, *54*, 11169-11186; (b) J. P. Perdew, K. Burke, M. Ernzerhof, *Phys. Rev. Lett.* **1996**, *77*, 3865-3868.

[5] G. Kresse, D. Joubert, Phys. Rev. B **1999**, 59, 1758-1775.

[6] H. J. Monkhorst, J. D. Pack, Phys. Rev. B **1976**, 13, 5188-5192.

[7] Z. Wang, G. Wang, H. Qi, M. Wang, M. Wang, S. Park, H. Wang, M. Yu, U. Kaiser, A. Fery, S. Zhou, R. Dong, X. Feng, *Chem. Sci.* **2020**, *11*, 7665-7671.

[8] X. Wu, Y. Qiu, Z. Chen, B. Guan, X. Hao, A. I. Rykov, Y. Sun, L. Liu, Y. Zou, J. Sun, W. Xu, D. Zhu, *Angew. Chem. Int. Ed.* **2020**, *59*, 20873-20878.

[9] J. Park, A. C. Hinckley, Z. Huang, D. Feng, A. A. Yakoyenko, M. Lee, S. Chen, X. Zou, Z. Bao, *J. Am. Chem. Soc.* **2018**, *140*, 14533-14537.

[10] G. Chen, L. B. Gee, W. Xu, Y. Zhu, J. S. Lezama Pacheco, Z. Huang, Z. Li, J. T. Babicz, Jr., S. Choudhury, T. H. Chang, E. Reed, E. I. Solomon, Z. Bao, *J. Am. Chem. Soc.* **2020**, *142*, 21243-21248.